Research Article

Tomasz Gałaj and Adam Wojciechowski

A study on numerical integration methods for rendering atmospheric scattering phenomenon

https://doi.org/10.1515/phys-2019-0025
Received Jan 29, 2019; accepted Mar 07, 2019

Abstract: A qualitative comparison of three, popular and most widely known numerical integration methods in terms of atmospheric single scattering calculations is presented. A comparison of Midpoint, Trapezoidal and Simpson's Rules taking into account quality of a clear sky generated images is performed. Methods that compute the atmospheric scattering integrals use Trapezoidal Rule. Authors try to determine which numerical integration method is the best for determining the colors of the sky and check if Trapezoidal Rule is in fact the best choice. The research does not only conduct experiments with Bruneton's framework but also checks which of the selected numerical integration methods is the most appropriate and gives the lowest error in terms of atmospheric scattering phenomenon.

Keywords: atmospheric single scattering, numerical integration, integrals, nonlinear light scattering, gpu rendering

PACS: 02.30.Rz, 42.68.-w

1 Introduction

Atmospheric scattering effects are very important for many applications that require high realism of the outdoor scenes. It becomes a crucial aspect affecting perception quality [1] of the contemporary games and virtual environments [2]. The sky color is a natural indicator of the time of a day. Recent methods such as [4, 6] calculate colors of the sky in real time (16ms). These methods use Trapezoidal Rule for integration the single scattering equation and then save this data into a precomputed look up table (LUT) as to retrieve it in a real time for image synthesis.

In this paper, a qualitative comparison of three, popular numerical integration methods to compute the single scattering integral is presented. In provided research, three methods have been chosen, namely Midpoint, Trapezoidal and Simpson's Rules. These three methods are fairly popular in Computer Graphics field. Atmospheric scattering is calculated using backward ray tracing algorithm taking into account variable light conditions [5]. Then, these methods are compared with each other taking into account quality of the generated images of the sky. As a subproduct of this research, the fidelity of the framework presented by Bruneton in [3] is being checked. Authors try to determine which numerical integration method is the best for calculating the colors of the sky and check if Trapezoidal Rule is in fact the best choice. This research does not only conduct experiments with Bruneton's framework but also checks which of the selected numerical integration methods is the most appropriate and gives the lowest error in terms of atmospheric scattering phenomenon.

2 Atmospheric scattering background

In this section, the physical background of atmospheric light scattering as well as mathematical model of this phenomenon is described.

2.1 Physical background

In computer graphics one can distinguish two types of light scattering – Rayleigh and Mie scattering. Rayleigh scattering occurs for particles much smaller than the wavelength of light and it can be described by Condition 1 [4].

$$r \ll \frac{\lambda}{4\pi} \tag{1}$$

Here r is a radius of particle (*e.g.* oxygen, carbon dioxide molecules), and λ is wavelength of light. On the other hand, when particles are bigger than λ, Rayleigh scattering smoothly transitions to Mie scattering. This type of scatter-

Tomasz Gałaj: Institute of Information Technology, Lodz University of Technology, Łódź, Poland; Email: tomasz.galaj@edu.p.lodz.pl
Adam Wojciechowski: Institute of Information Technology, Lodz University of Technology, Łódź, Poland; Email: adam.wojciechowski@p.lodz.pl

ing considers aerosols as well as small steam, ice, dust particles.

The major difference between these two types of scattering is that intensity of Rayleigh scattering depends on the wavelength of scattered light, whereas Mie scattering does not. This implies that the blue sky color is the effect of Rayleigh scattering combined with a lack of violet photon receptors in people's retinas [7]. On the other hand, the grey tones of halos around the sun, clouds, fog are caused by Mie scattering.

What is more, one has to define single and multiple scattering terms. Single scattering means that only one light scattering event [8] is taken into account – event after which some part of light traveling towards the eye is deflected away from the viewing direction (out-scattering) or is deflected back on the viewing direction (in-scattering). On the other hand, with multiple scattering a number of light scattering events are taken into account. In this research only the single scattering term is taken into account as it is less complex than multiple scattering and it is sufficient in terms of verification of the stated hypothesis.

2.2 Mathematical model

In this section equations of physically based mathematical model are presented that were used to calculate single atmospheric scattering. The equations are based on the ones that were proposed by Nishita [4, 9].

2.2.1 Scattering intensity

Scattering intensity for Rayleigh/Mie scattering is described by Equation 2. It expresses the amount of light that has been scattered exactly at a point P (see Figure 1) towards direction $\vec{V}$ and with incident light direction $\vec{L}$.

$$I_{S_{R,M}}(\lambda, \theta, P) = I_I(\lambda)\rho_{R,M}(h)F_{R,M}(\theta)\beta^s_{R,M}(\lambda) \tag{2}$$

In the above equation, λ is the spectral wavelength of the light, $I_I(\lambda)$ stands for the spectral intensity of the incoming light [10], $\rho_{R,M}(h)$ is the Rayleigh/Mie density function, $F_{R,M}(\theta)$ is phase function for the angle θ between $\vec{V}$ and $\vec{L}$, and $\beta^s_{R,M}(\lambda)$ is scattering coefficient.

The density function $\rho_{R,M}(h)$ expresses how density of air particles decreases in dependence of altitude h. This function is defined by Equation 3.

$$\rho_{R,M}(h) = \exp(-\frac{h}{H_{R,M}}) \tag{3}$$

In the above equation, h is the altitude of the point P above the ground and $H_{R,M}$ are scale heights for Rayleigh and Mie scattering respectively. Proposed solution uses $H_R = 8000m$ and $H_M = 1200m$ as Bruneton *et al.* suggested in [6].

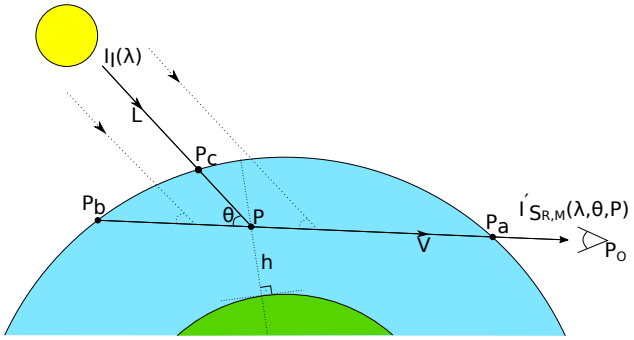

Figure 1: Schematic of how the single scattering is being calculated. The amount of light that enters the viewer's eye along viewing direction $\vec{V}$ (from P_a to P_b) is integrated. When viewer is inside the atmosphere then $P_a = P_O$. Next, incoming light $\vec{L}$ enters the atmosphere at point P_C. Then the amount of light from the sun (from P to P_C) that reaches point P (at altitude h) along viewing direction $\vec{V}$ is integrated

2.2.2 Scattering coefficients

Rayleigh's scattering equation provides scattering coefficients for a volume for which we know its molecular density. These coefficients are given by Equation 4.

$$\beta^s_R(\lambda) = \frac{8\pi^3(n^2-1)^2}{3N\lambda^4} \tag{4}$$

Here superscript S indicates that it is a scattering coefficient, subscript R means that it is a coefficient for Rayleigh scattering, λ is the given light's wavelength, n is index of refraction of air and N is molecular density at sea level. As one can see, this equation depends on the wavelength. If the wavelength is short, the value of β^s_R will be higher and if the wavelength is long, the value of β^s_R will be lower.

This explains why the sky is blue during the day and red-orange at the dawn or dusk. During the day, when the sun is in the zenith, light has relatively short distance to travel before reaching observer's eye and therefore blue light is being scattered towards the eye and sky appears blue (green and red light need to travel bigger distance to be scattered). On the other hand, at sunrise or sunset, light has to travel much longer distance than in the previous scenario. Before light reaches the observer's eye, most of the blue light has been scattered away, and only red-green light will have a chance to reach observers eye.

Mie scattering is similar to Rayleigh, but it applies to particles that are much greater than the scattered wavelength. These particles (aerosols) may be found on low altitudes of the Earth's atmosphere. Therefore, equation for Mie scattering coefficients needs to be slightly different (Equation 5).

$$\beta_M^s() = \frac{8\pi^3(n^2-1)^2}{3N} \tag{5}$$

Here subscript M stands for Mie scattering and the rest of the parameters are the same as in the Rayleigh scattering coefficient equation.

2.2.3 Phase functions

The phase function is describing angular dependency of scattered light in respect to the direction of incoming light when its ray collides with a particle. This function takes as a parameter angle θ which is the angle between scattered light ray and incoming light ray. The result of this function reflects the amount of light that has been scattered. Equations 6 and 7 show phase functions for Rayleigh and Mie scattering respectively that were used in proposed solution.

$$F_R(\theta) = \frac{3}{16\pi}(1+\cos^2(\theta)) \tag{6}$$

$$F_M(\theta) = \frac{3}{8\pi}\frac{(1-g^2)(1+\cos^2(\theta))}{(2+g^2)(1+g^2-2g\cos(\theta))^{\frac{3}{2}}} \tag{7}$$

Here parameter $g \in (-1;1)$ is an asymmetry factor which describes the anisotropy of the medium (if it is forward or backward scattering). It should be noted that Mie phase function [11] is very complex and can not be computed using single analytic function. What is shown in Equation 7 is Henyey-Greenstein's approximation of the Mie phase function, which is used in proposed solution.

2.2.4 Optical depth

Optical depth, or transmittance expresses how much the light is being attenuated after traveling the distance $|P_b - P_a|$ in a medium. Equation 8 defines the transmittance.

$$t(P_a, P_b, \lambda) = \beta_{R,M}^s(\lambda)\int_{P_a}^{P_b} e^{\frac{-h(P)}{H_{R,M}}}\,dP \tag{8}$$

Parameter λ is the wavelength of attenuated light. Optical depth attenuation is the effect of out-scattering in participating media.

2.2.5 Single scattering

In previous sections all the components that are required to compute the single scattering have been introduced. To compute single scattering, Equation 9 that takes into account Rayleigh and Mie scattering is used. This equation defines the single scattering intensity of the light beam that reaches the observer's eye, after exactly one scattering event.

$$I'_{S_{R,M}}(\lambda,\theta,P) = I_I(\lambda)\beta_{R,M}^s(\lambda)F_{R,M}(\theta)\int_{P_a}^{P_b}(\rho_{R,M}(h(P))\cdot e^{-t(P,P_c,\lambda)-t(P,P_a,\lambda)})dP \tag{9}$$

In the Equation 9, the term P_O is location of the observer's eye, $\vec{L}$ is the direction from the light source to sample point P on $\vec{V}$, λ is the wavelength of the scattered light. Point P is the sample point at altitude h. P_a is the point where ray from observer's position (P_O) enters the atmosphere along the viewing direction $\vec{V}$. P_b is the point where the ray from observer's position exits the atmosphere or hits the ground. P_c is the intersection point of $\vec{L}$ and the atmosphere before reaching point P. Note that if the observer is inside the atmosphere then $P_o = P_a$ (origin of the ray from the observer's position is already inside the atmosphere). It is also assumed that all light rays that come to sample points along $\vec{V}$ (*e.g.* point P) are parallel.

The final intensity of single scattered light I'_S is obtained by the sum of single scattering for Rayleigh and Mie. It is described by Equation 10.

$$I'_S = I'_{S_R} + I'_{S_M} \tag{10}$$

2.3 Selected numerical integration methods

Three the most widely used numerical integration methods have been selected, namely Trapezoidal, Midpoint and Simpson's Rules [12]. These methods are used to compute the single scattering integral (Equation 9) inside the atmosphere.

Trapezoidal Rule approximates area under a function as a trapezoid (straight line segments). Then area of the trapezoid is being calculated. This method may be also defined as averaging left and right Riemann Sums. Trapezoidal Rule is used by most of the methods computing atmospheric scattering integrals.

On the other hand, Midpoint Rule approximates a region under a function as a rectangle and then computes its area. It should be noted that this method generates (generally) bigger numerical error than the Trapezoidal Rule.

The last considered method is Simpson's Rule. This method approximates definite integral of a function using parabolic arcs (quadratic polynomials). In this rule area under parabolas are being calculated.

More on different numerical integration methods can be found in [12].

3 Related work

One of the first papers tackling the subject of simulating atmospheric scattering was [9]. Nishita *et al.* presented a method for calculating atmospheric scattering taking into account Rayleigh and Mie single scattering. Their method was based on a set of physically based equations (Nishita's model), shown in the previous section, for calculating single scattering in the atmosphere. This method does not enable user to change interactively atmosphere's density (*e.g.* to visualize different planet's sky or to distinguish dawn from dusk) due to precomputed values stored in a lookup table. The model presented by Nishita *et al.* was a basis for most atmospheric scattering research in the field of computer graphics.

Another, the most widely used model is Preetham's model [13] introduced in 1999. Unlike Nishita's model, this is an analytical model. It was obtained by computing the sky radiances for many view and sun directions and different turbidity values using Nishita' model and then they used nonlinear least square fitting algorithm. Therefore, his solution was able to calculate colors of the sky in real time, but had many major drawbacks as was pointed in [14]. In some specific conditions Preetham's model was giving negative values of intensity and under some circumstances the model was behaving incorrectly (this model breaks down numerically and has unrealistic luminance distribution [3, 14]).

In 2005, O'Neil [15] presented one of the first implementations of atmospheric scattering on GPU. To be able to implement this phenomenon on GPU he had to simplify Nishita's model [9]. He presented a set of analytic functions that he used for computing color of the sky. His solution was able to perform integration in real time per vertex instead of per pixel [16] as he was conducting all of the calculations in Vertex Shader [17, 18].

The first method that used precomputed single scattering values in real time was Schafhitzel *et al.* [19]. The authors succeeded to precompute single scattering equations in a big 3D lookup table as O'Neil suggested [15]. However, this 3D texture lacked one dimension as authors did not take into account multiple scattering.

In 2008, Bruneton *et al.* [6] presented a method that based on Schafhitzel's work. They presented the first real time method that was taking into account multiple scattering and they successfully precomputed single and multiple scattering terms in a 4D lookup table. Their method was working for all viewing directions and virtual camera positions at the daytime.

In 2009, Elek [4] presented a quick and memory efficient atmospheric scattering method. He based his method on the work of Schafhitzel *et al.* [19]. He managed to reduce the dimensionality of the 4D multiple scattering LUT to 3D LUT while keeping the quality of Bruneton's method [3].

The main drawback of Elek's and Bruneton's method is that texel fetches from 4D or even 3D lookup tables are very expensive operations (in terms of efficiency) [20].

What is more, all of the before mentioned methods have one thing in common. They all use the same numerical integration method which is the Trapezoidal Rule. One may believe, that enhancing or carefully selecting numerical integration method will lead to obtaining better results with the above methods. What is more, an in depth investigation of numerical integration methods may lead to developing a desired method that could calculate the single scattering integral with the lowest possible error in real time without the precomputation step. Furthermore, the state of the art methods are also fairly complex to implement in a real life project/game, since they use some tricks/hacks that have a strong impact on how these methods perform.

In the presented research, emphasis was put mainly on single scattering approach since it is less complex than multiple scattering and provides reliable verification of research hypothesis.

4 Numerical integration algorithms' comparison methodology

To compare the selected numerical integration methods a framework was used that was developed by Bruneton [3]. This framework was initially used to qualitatively and quantitatively compare 8 clear sky rendering methods which were created over the years. What this framework does is it compares each method with each other as well as with measurements (measured by Kider *et al.* [21]) and with reference model from physics community (libRadtran). During comparison with the ground truth, the framework generates Root Mean Square Error (RMSE) between the current method and the method based on measurements. What is more, it also generates a set of images (skydome renders, absolute and relative luminance, chro-

maticity and the relative error compared with the method based on measurements) for different times of day. The framework runs each method for the same atmospheric parameters.

The framework was not modified itself, but only the methods that used the chosen numerical integration algorithms to calculate the single scattering equations have been added. Selected numerical integration methods have been compared in three cases where each case had different number of integration steps (see Table 1).

Table 1: Each selected numerical integration method is being compared in three cases where each case has different number of integration steps

Case	Samples on $\vec{V}$	Samples on $\vec{L}$
Low quality	16	8
Medium quality	128	64
High quality	512	256

5 Results

It was decided to divide the experiments into three cases. Each case had different number of the integration samples. All cases and their corresponding number of used integration samples are presented in Table 1.

Using the above mentioned framework, a set of results for each case has been generated, where each set consists of:

- Fisheye skydome renders,
- Absolute luminance figures,
- Relative luminance figures,
- Chromaticity figures,
- Relative error figures,
- RMSE value.

The reference method used by the Bruneton's framework is method based on measured sky data [21] which is labelled as Measurements in the following images. It should be noted that all the figures have been generated for the purpose of this research using the aforementioned framework.

5.1 Fisheye skydome renders

Fisheye skydome renders of the spectral radiance, presented in Figure 2, were obtained for each numerical in-

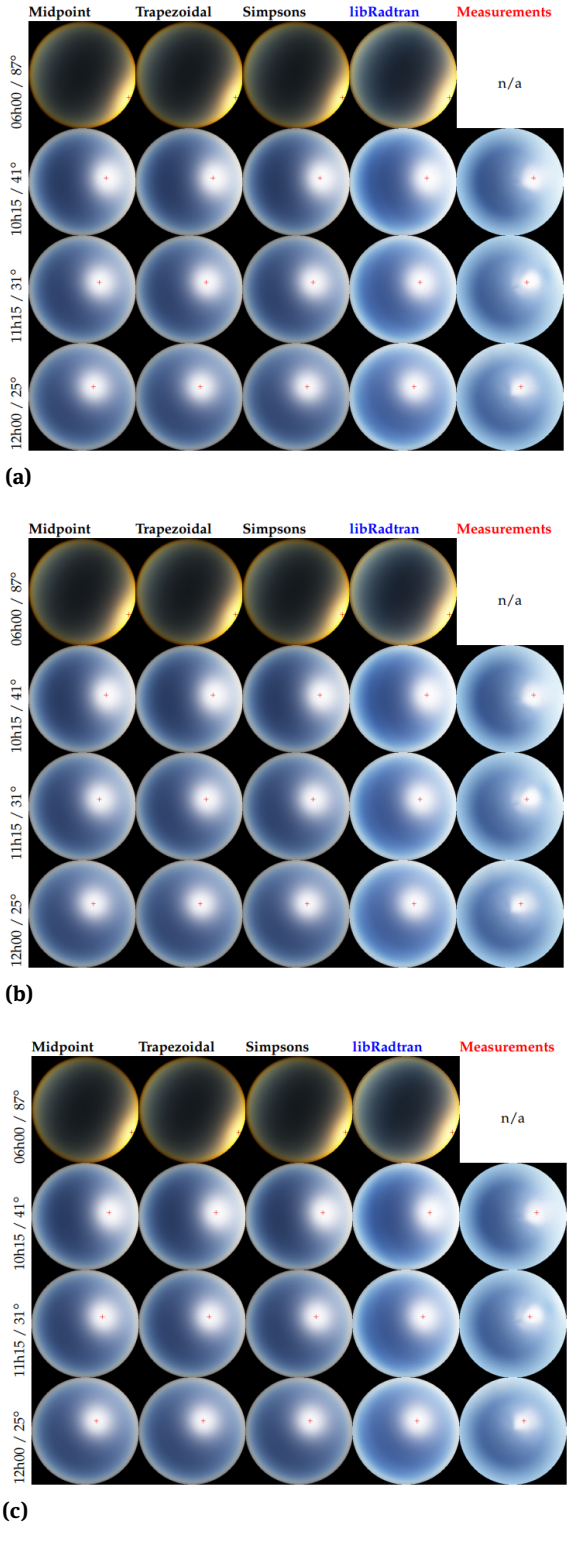

Figure 2: Fisheye skydome renders of the spectral radiance obtained for each numerical integration method for each considered case: a) case 1 – low quality, b) case 2 – medium quality, c) case 3 – high quality

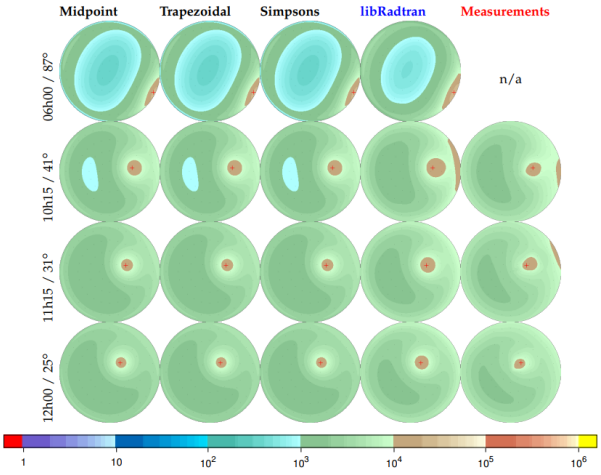

(a)

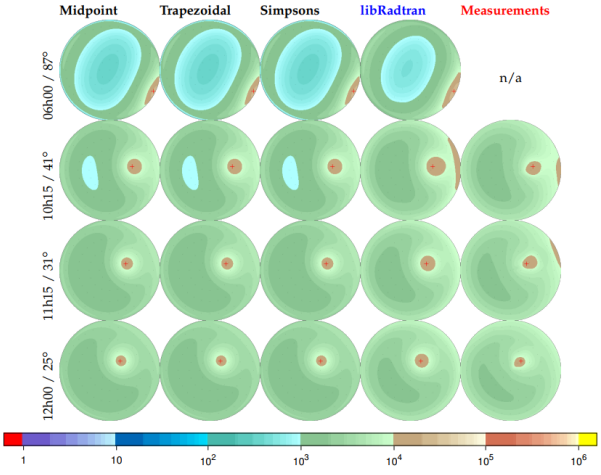

(b)

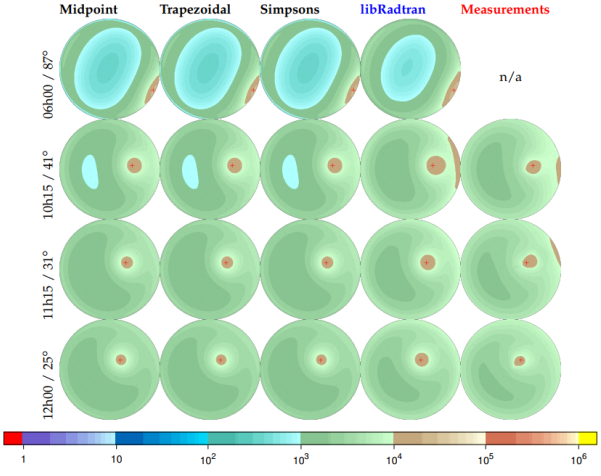

(c)

Figure 3: The absolute luminance in $cd.m^{-2}$ was obtained for each numerical integration method for each considered case: a) case 1 – low quality, b) case 2 – medium quality, c) case 3 – high quality

tegration method, convolved with the CIE color matching functions, converted from XYZ to linear sRGB and finally tone mapped using $1 - e^{-kL}$ function [3]. These images were rendered for several times of day/sun zenith angle values. The red cross indicates the sun direction. The measurements were interpolated using bicubic spherical interpolation before rendering [21].

In the Figure 2 one can see that Trapezoidal Rule generates visibly darker skydomes than the other methods ($sun\ zenith\ angle = 87°$). Moreover, the color at the horizon (boundaries) is more orange/yellow than the reference skydome generated by libRadtran and other integration methods.

What is more, Trapezoidal and Simpson's Rules generates highlight with bigger radius than the method based on measurements or libRandtran ($sun\ zenith\ angle = 25°$). One can notice that all selected numerical integration methods generate renders that are too dark when compared to references images (libRadtran and measurements).

5.2 Absolute luminance

The absolute luminance in $cd.m^{-2}$ was obtained for each numerical integration method, using the same color scale as in [14] (logarithmic scale in cd/m^2). The measurements were interpolated using bicubic spherical interpolation before being converted to luminance values.

In Figure 3 one can notice that Trapezoidal Rule method in case 1 (low quality) generates the worst luminance values where $sun zenith angle = 87°$. Furthermore, one can see, that Simpson's Rule gives the lowest luminance difference in all cases when compared to the reference methods.

5.3 Relative luminance

The relative luminance obtained for each numerical integration method, in percentage of the zenith luminance. The same color scale was used as in [14] (logarithmic scale in percent of zenith luminance). The measurements were interpolated using bicubic spherical interpolation before being converted to luminance values.

When one takes a closer look at the last row in Figure 4 (for all cases), it can be noticed that for the low quality case, Trapezoidal and Simpson's Rules are giving better relative luminance values than for the higher quality cases. When it comes to Midpoint Rule, relative luminance vaules are better in the higher quality cases.

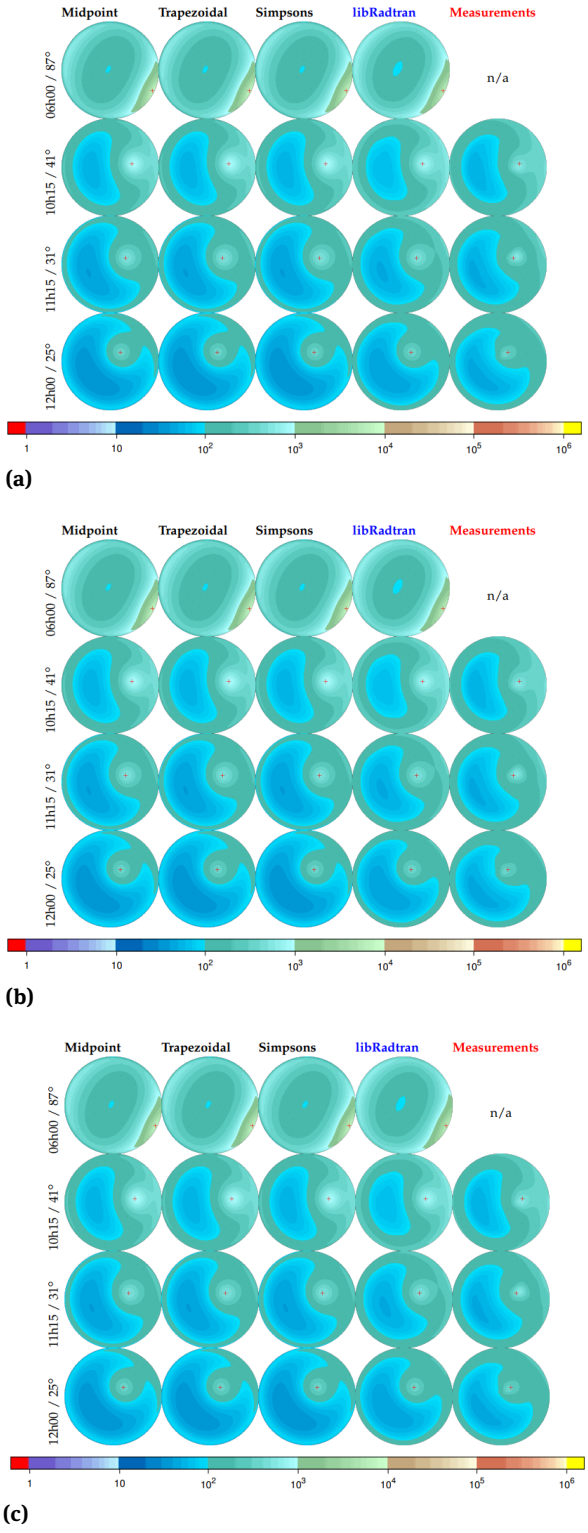

Figure 4: The relative luminance obtained for each numerical integration method for each considered case: a) case 1 – low quality, b) case 2 – medium quality, c) case 3 – high quality

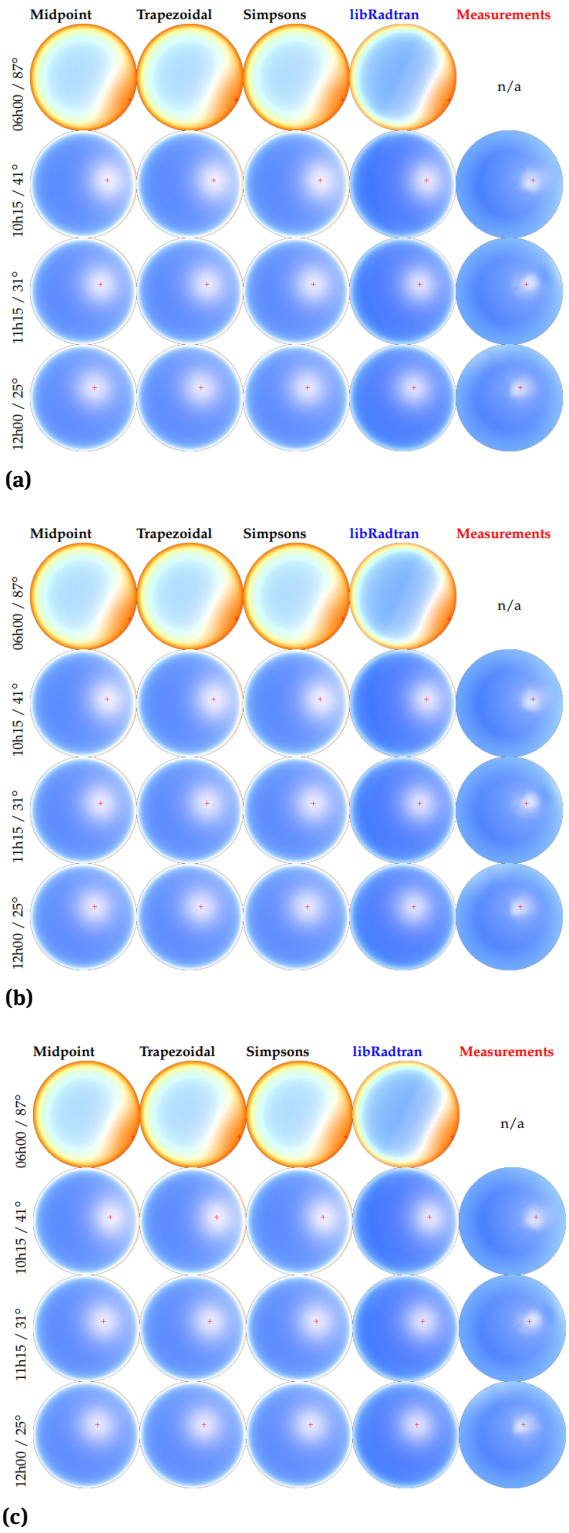

Figure 5: The rg-chromaticity, $(r, g, b)/\max(r, g, b)$, computed for each numerical integration method for each considered case: a) case 1 – low quality, b) case 2 – medium quality, c) case 3 – high quality

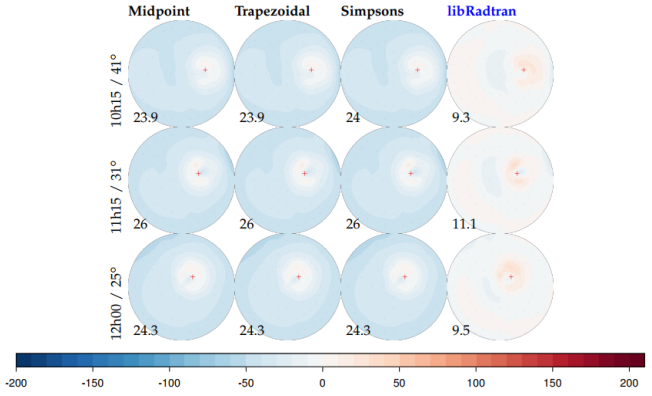

(a)

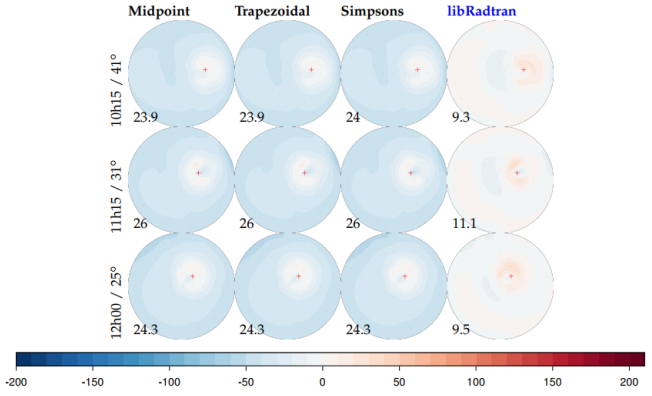

(b)

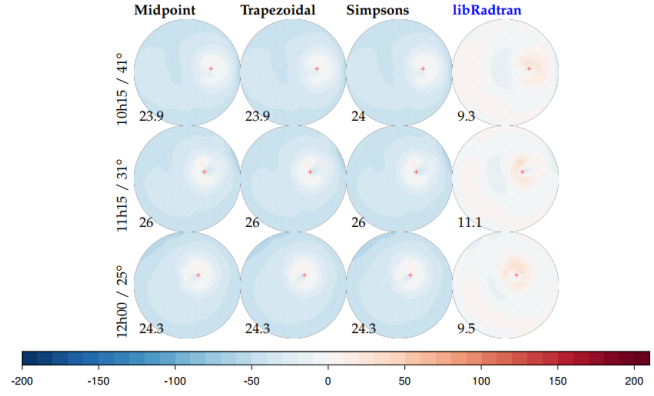

(c)

Figure 6: The relative error compared with the measurements (in %) computed for each numerical integration method for each considered case: a) case 1 – low quality, b) case 2 – medium quality, c) case 3 – high quality

5.4 Chromaticity

The rg-chromaticity, $(r, g, b)/\max(r, g, b)$ [3], was computed for each numerical integration method. The measurements were interpolated using bicubic spherical interpolation before being converted to chromaticity values.

Table 2: The resulting RMSE values in $mW/(m^2 \cdot sr \cdot nm)$ for each selected numerical integration method for each considered case.

	Method	RMSE $mW/(m^2 \cdot sr \cdot nm)$
Case 1 low quality	Midpoint	32.2
	Trapezoidal	33.7
	Simpsons	31.3
Case 2 medium quality	Midpoint	26.3
	Trapezoidal	26.2
	Simpsons	26.4
Case 3 high quality	Midpoint	25.6
	Trapezoidal	25.6
	Simpsons	25.6

Looking at chromaticity values (Figure 5), for all the selected methods one can notice orange color at the horizon (boundaries) which should not be there – this is the area where the biggest rendering artifacts occur. It also can be noticed that for medium and high quality cases this orange color at the horizon is slowly fading out.

5.5 Root mean square error

Here, the root mean square error relative to the measurements is predented, in % and using the same color scale as in [21], computed at the 81 sampling points (and summed equally over the common range supported by all methods, *i.e.* between 360 and 720 nm), and then interpolated with spherical bicubic interpolation. The bottom left numbers in Figure 6 is the RMSE in $mW/(m^2 \cdot sr \cdot nm)$ for different sun zenith angles.

When one takes a look at the Figure 6 and Table 2 where the RMSE values are presented, it can be noticed that for lower number of samples the result is much worse than for bigger number of samples. This is especially visible for the low quality case (Figure 6a for Trapezoidal Rule), where the relative error is the biggest among the selected methods. On the other hand, for the lowest number of samples, the most accurate method was the Simpson's Rule.

However, when one takes larger number of samples (case 2 – medium quality) one may see that the lowest error was obtained by Trapezoidal Rule, but it is not very different than for the other selected methods.

Looking at the third case (high quality), where the number of samples was the highest, all of the selected methods obtained the same RMSE.

It can be noticed, that overally all of the selected numerical integration methods underestimate the relative error.

6 Conclusions

From the above results it can be told, that all the selected methods perform almost the same. Midpoint and Simpson's Rules are best when one would like to use lower number of samples. Trapezoidal Rule is better when using bigger number of samples (case 2 – medium quality). Last but not least, when one can use arbitrary number of samples (case 3 – high quality) to, for example, precompute some parts of the single scattering integral (Equation 9), any of the selected methods will give accurate results, that should not affect the final image.

Moreover, the Bruneton's framework is a very good tool to compare the various atmospheric scattering methods with each other. It may be very helpful during the development of a new method to compute atmospheric scattering phenomena.

References

[1] Fornalczyk K., Napieralski P., Szajerman D., Wojciechowski A., Sztoch P., Wawrzyniak J., Stereoscopic image perception quality factors, Mixed Design of Integrated Circuits & Systems (MIXDES), 2015 22nd International Conference, IEEE, 2015, 129-133.

[2] Wojciechowski A., Camera navigation support in a virtual environment, Bulletin of the Polish Academy of Sciences: Technical Sciences, 2013, 61, 871-884.

[3] Bruneton E., Neyret F., Precomputed atmospheric scattering, Computer Graphics Forum, Wiley Online Library, 2008, 27, 1079-1086.

[4] Elek O., Rendering parametrizable planetary atmospheres with multiple scattering in real-time, Proceedings of the Central European Seminar on Computer Graphics, Citeseer, 2009.

[5] Forczmański P., Kukharev G., Shchegoleva N., Simple and Robust Facial Portraits Recognition under Variable Lighting Conditions Based on Two-Dimensional Orthogonal Transformations, A. Petrosino, ed., Image Analysis and Processing – ICIAP 2013, Springer Berlin Heidelberg, Berlin, Heidelberg, 2013, 602-611.

[6] Bruneton E., A Qualitative and Quantitative Evaluation of 8 Clear Sky Models, IEEE transactions on visualization and computer graphics, 2017, 23, 2641-2655.

[7] Gibbs P., Why is the sky blue?, Original Usenet Physics FAQ, Retrieved October, 1997.

[8] Jarosz W., Efficient Monte Carlo methods for light transportin scattering media, Citeseer, 2008.

[9] Nishita T., Sirai T., Tadamura K., Nakamae E., Display of the earth taking into account atmospheric scattering, Proceedings of the 20th annual conference on Computer graphics and interactive techniques, ACM, 1993, 175-182.

[10] Stair R., Johnston R.G., Bagg T.C., Spectral distribution of energy from the sun, Journal of Research of the National Bureau of Standards, 1954, 53, 113-119.

[11] Frisvad J.R., Christensen N.J., Jensen H.W., Computing the scattering properties of participating media using Lorenz-Mietheory, ACM Transactions on Graphics (TOG), 2007, 26, 60.

[12] Davis P.J., Rabinowitz P., Methods of numerical integration, Courier Corporation, 2007.

[13] Preetham A.J., Shirley P., Smits B., A practical analytic model for daylight, Proceedings of the 26th annual conference on Computer graphics and interactive techniques, ACM Press/Addison-Wesley Publishing Co., 1999, 91-100.

[14] Zotti G., Wilkie A., Purgathofer W., A critical review of the Preetham skylight model, WSCG International Conference in Central Europe on Computer Graphics, Short Communications Papers Proceedings, 2007.

[15] O'Neil S., Accurate atmospheric scattering, GPU Gems, 2005, 2, 253-268.

[16] Jelliti I., Romanowski A., Grudzien K., Design of crowdsourcing system for analysis of gravitational flow using x-ray visualization, Computer Science and Information Systems (FedCSIS), 2016 Federated Conference, IEEE, 2016, 1613-1619.

[17] Lipiński P., On domain selection for additive, blind image watermarking, Bulletin of the Polish Academy of Sciences: Technical Sciences, 2012, 60, 317-321.

[18] Puchala D., Approximating the KLT by maximizing the sum of fourth-order moments, IEEE Signal Processing Letters, 2013, 20, 193-196.

[19] Schafhitzel T., Falk M., Ertl T., Real-time rendering of planets with atmospheres, WSCG International Conferencein Central Europe on Computer Graphics, Visualization and Computer Vision, 2007.

[20] Lengyel E., Game Engine Gems 2, EBL-Schweitzer, CRCPress, 2011.

[21] Kider Jr J.T., Knowlton D., Newlin J., Li Y.K., Greenberg D.P., A framework for the experimental comparison of solar and skydome illumination, ACM Transactions on Graphics(TOG), 2014, 33, 180.